The effect of Sn doping on the electronic and mechanical properties of $Ti_3Al_{1-x}Sn_xC_2$ MAX phases

Ayşenur GENCER[1],[*] ⬤, **Aytaç ERKİŞİ**[2] ⬤

[1]Department of Physics, Kamil Özdağ Faculty of Science, Karamanoğlu Mehmetbey University, Karaman, Turkey
[2]Department of Physics, Faculty of Art and Sciences, Pamukkale University, Denizli, Turkey

Abstract: The phase pure synthesis of Ti_3AlC_2 MAX phase is quite difficult and some additives are required to get a phase pure Ti_3AlC_2 such as Sn. In this study, Sn doped Ti_3AlC_2 MAX phase has been investigated taking into account the experimental synthesis conditions where some Sn atoms could replace Al atoms in the structure. For this purpose, $Ti_3Al_{1-x}Sn_xC_2$ with x ranging from 0 to 1 with 0.1 interval has been studied using the first principles method and the results show that all compositions are thermodynamically stable. The electronic properties of these compositions have been studied using band filling theory in detail. Also, the mechanical properties of these compounds such as shear modulus, Poisson's ratio, Young's modulus, sound wave velocities, polarization of the sound waves, enhancement factor, the power flow angle and etc. have been obtained with the varying directions and the three-dimensional mechanical properties have been visualized.

Key words: MAX phases, nanolaminated ternary carbides, electronic stability, anisotropic elastic, density functional theory

1. Introduction

The MAX phases belong to the nanolaminated ternaries, having the general formula $M_{n+1}AX_n$ *(n=1-3)* where M is an early transition metal, A is an A group element, and X is either carbon or nitrogen [1]. They are also known as 211 (*n = 1*), 312 (*n = 2*) and 413 (*n = 3*) *MAX* phases due to the *n values*. Each of three phases crystallizes in a hexagonal $P6_3/mmc$ lattice structure and they consist of edge-sharing [*M6X*] octahedra interleaved with A layers. Hence, their unique structure, combining both strong covalent *M-X* bonds and weaker *M-A* bonds, makes *MAX* phase having magnificent properties. They are stiff, lightweight, chemically stable, and oxidation resistant. On the other hand, they are relatively soft, machinable, resistant to thermal shock, and they exhibit good electric and thermal conductivity as well as good damage tolerance. Therefore, they exhibit both ceramic and metallic nature [1–4]. Among these *MAX* phases, Ti_3AlC_2 has the desirable attention owing to their unique combination of electrical, thermal, chemical and mechanical properties [5–8]. To synthesize Ti_3AlC_2 many experimental techniques such as sintering [9–11], combustion synthesis [12], hot pressing [8,13,14] have been used from various mixtures with different molarities. Whereas, obtaining Ti_3AlC_2 in a single-phase is quite difficult due to the narrow phase domain in the Ti–Al–C phase diagram [15]. The earlier studies revealed that secondary phases such as TiC, Ti_xAl_y, Al_2O_3, or the *211 MAX* phase (Ti_2AlC) are commonly detected in the end products [16–18]. In addition, there are two main problems for the large-

---

*Correspondence: aysenurgencer@gmail.com

scale production of highly pure Ti_3AlC_2 powders. These challenges are the evaporative loss of Al and the thermal explosion in the reaction process of Ti–Al–C. In order to prevent these problems some additives such as B_2O_3, Si and Sn were introduced to Ti–Al–C system [5,9,19,20]. It was observed that evaporative loss of Al could be supplemented by the Sn additions. Hence, Sn addition would solve the evaporative loss of Al and the thermal explosion simultaneously, and does not remain as impurities in the product of Ti_3AlC_2 powders [5]. Moreover, the experimental studies have considered the $Ti_3Al_{0.8}Sn_{0.2}C_2$ compound for the hardness [15], oxidation resistance [18], and compressive behavior [21] as well as with Ti_3AlC_2. However, there is a lack for the detailed properties of Sn doped Ti_3AlC_2 in the literature. Therefore, $Ti_3Al_{1-x}Sn_xC_2$ compounds were considered where x starts from 0 and increases to 1 with 0.1 interval and the detailed structural, electronic and mechanic properties of $Ti_3Al_{1-x}Sn_xC_2$ compounds are presented in this study.

2. Computational details

$Ti_3Al_{1-x}Sn_xC_2$ compounds were investigated using Cambridge Serial Total Energy Package (CASTEP) [22] based on the density functional theory (DFT). The exchange correlation energy was considered using the Perdew–Burke–Ernzerhof (PBE) [23] functional within the generalized gradient approximation (GGA) [24]. Also, the self-consistent field calculations were performed using the Broyden–Fletcher–Goldfarb–Shannon (BFGS) method [25]. The electron and ion interactions were considered using the norm-conserving pseudopotentials [26]. The optimizations were performed with an energy cut off as 770 eV and with $14 \times 14 \times 2$ k-points. The electron configurations within the virtual crystal approximation (VCA) [27] were used as $4d^2 4s^2$, $3s^2 3p^1$, $5s^2 5p^2$, and $2s^2 2p^2$ for Ti, Al, Sn, and C atoms, respectively. For the structural optimization, the energy and force criteria were taken as 5×10^{-7} eV per atom and 0.001 eV/Å, respectively. The three-dimensional and two-dimensional elastic properties were modeled using ELATE [28]. Also, the Christoffel tool [29] were used to obtain the three-dimensional sound wave velocities with solving the Christoffel equation [30].

3. Results and discussion

3.1. Structural and electronic properties

Titanium aluminum carbides $Ti_3Al_{1-x}Sn_xC_2$ (where x is ranging from 0 to 1 with interval 0.1) in which tin element (Sn) is doped in different proportions were modelled according to the hexagonal symmetry. The crystallized structure conforming to $P6_3/mmc$ space group is illustrated in Figure 1.

The relaxation process of each composition having different stoichiometry was carried out to obtain the optimized lattice parameters and ground state energies. The obtained lattice constants (a and c in Å), bond lengths (d in Å) and also formation energies $(\Delta E_{For}$ in eV/atom$)$ for each composition were tabulated in Table 1. As can be concluded from Table 1, the total unit cell volume of each composition having various Sn addition changes due to the doping rate. Once compared the obtained lattice parameters in the present study with the previous experimental and theoretical studies for Ti_3AlC_2, $Ti_3Al_{0.8}Sn_{0.1}C_2$ and Ti_3SnC_2 compositions, the results are coherent and only about 1% gap is found between them [15,18]. Moreover, the general trend for the a and c lattice parameters is raising with the x ratios changes from 0 to 1 and Ti_3SnC_2 has the highest lattice parameter among these compositions. This result is due to the higher atomic radius of Sn atom than Al atom. In addition, the formation energies were calculated for each composition of $Ti_3Al_{1-x}Sn_xC_2$ with the help of internal energy changes [4,31] and they were found to be negative values which point the structural stability of compositions.
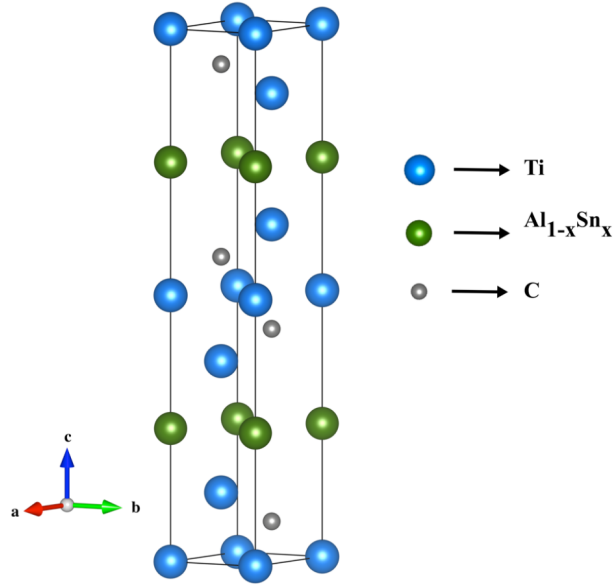
Figure 1. The three-dimensional crystal structure of Sn-doped $Ti_3Al_{1-x}Sn_xC_2$.

Table 1. The obtained lattice constants (a and c in $Å$), bond lengths (d in $Å$) and formation energies (ΔE_{For} in $eV/atom$) for each composition.

Composition	a	c	ΔE_{For}	d_{Ti-C}	d_{Ti-Ti}	d_{Ti-TM}
Ti_3AlC_2	3.079	18.595	−0.840	2.079	2.967	2.886
	3.075[18]	18.572[18]				
	3.079[15]	18.589[15]				
	3.081*	18.679*	−0.763*			
$Ti_3Al_{0.9}Sn_{0.1}C_2$	3.083	18.525	−0.792	2.077	2.955	2.887
$Ti_3Al_{0.8}Sn_{0.2}C_2$	3.088	18.546	−0.765	2.078	2.954	2.895
	3.084[18]	18.587[18]				
	3.084[15]	18.621[15]				
$Ti_3Al_{0.7}Sn_{0.3}C_2$	3.092	18.557	−0.682	2.079	2.953	2.901
$Ti_3Al_{0.6}Sn_{0.4}C_2$	3.097	18.563	−0.649	2.081	2.952	2.907
$Ti_3Al_{0.5}Sn_{0.5}C_2$	3.102	18.567	−0.643	2.090	2.972	2.892
$Ti_3Al_{0.4}Sn_{0.6}C_2$	3.107	18.567	−0.655	2.085	2.950	2.917
$Ti_3Al_{0.3}Sn_{0.7}C_2$	3.123	18.571	−0.684	2.091	2.953	2.926
$Ti_3Al_{0.2}Sn_{0.8}C_2$	3.118	18.573	−0.713	2.089	2.950	2.926
$Ti_3Al_{0.1}Sn_{0.9}C_2$	3.123	18.567	−0.748	2.092	2.951	2.928
Ti_3SnC_2	3.142	18.695	−0.841	2.097	2.960	2.957
	3.150*	18.733*	−0.785*			

*Materials Project (2020). mp-3747: Ti_3 [online].
Website https://materialsproject.org/materials/mp-3747/ and mp-21023: Ti_3[online].
Website https://materialsproject.org/materials/mp-21023/ [accessed 29 December 2020].

The electronic stability of the crystals can be deduced with the density of states (DOS) plots which are obtained by using the band filling theory [32–36]. Therefore, after the optimization process, the electronic band structures and the total density of states (DOS) were investigated in order to determine the electronic properties of each $Ti_3Al_{1-x}Sn_xC_2$ compounds and get the best structural stoichiometry among them.

According to the theory in question, the structural stability is related to the ratio of the width of occupied states (W_{occ}) to the width of the bonding states (W_b) and when the mentioned ratio (W_{occ}/W_b) is close to 1, it can be said that the examined solid crystal has structural stability. In this study, it can be deduced from Table 2 that the calculated W_{occ}/W_b is much close to 1.00 value when the doping ratio of tin element inside of titanium aluminum carbides $Ti_3Al_{1-x}Sn_xC_2$ is 0.2. It means that this composition has better structural stability than the other compositions. Also, Table 2 lists the number of electrons at the Fermi level for each composition and $Ti_3Al_{0.8}Sn_{0.2}C_2$ has the lowest number of electrons among them. Therefore, $Ti_3Al_{0.8}Sn_{0.2}C_2$ is electronically more stable. These numbers of electrons could be visualized with the total DOS and Figure 2 shows the total DOS of these compounds where the inset shows that the lowest numbers of electrons are belongs to $Ti_3Al_{0.8}Sn_{0.2}C_2$ compound.

Table 2. Number of electrons at the Fermi level (n), the width of pseudo-gap (W_p), the width of occupied states (W_{occ}), the width of the bonding states (W_b), and the ratio of the width of the occupied states to the width of the bonding states (W_{occ}/W_b) for $Ti_3Al_{1-x}Sn_xC_2$ compositions.

| Compositions	n	W_p	W_{occ}	W_b	W_{occ}/W_b
Ti_3AlC_2	3.566	0.059	12.672	−12.613	−1.005
$Ti_3Al_{0.9}Sn_{0.1}C_2$	3.481	0.032	12.663	−12.630	−1.003
$Ti_3Al_{0.8}Sn_{0.2}C_2$	3.340	−0.030	12.045	−12.075	−0.998
$Ti_3Al_{0.7}Sn_{0.3}C_2$	3.386	−0.136	12.564	−12.700	−0.989
$Ti_3Al_{0.6}Sn_{0.4}C_2$	3.378	−0.187	12.533	−12.720	−0.985
$Ti_3Al_{0.5}Sn_{0.5}C_2$	3.427	−0.276	12.470	−12.746	−0.978
$Ti_3Al_{0.4}Sn_{0.6}C_2$	3.421	−0.374	12.406	−12.780	−0.971
$Ti_3Al_{0.3}Sn_{0.7}C_2$	3.632	−0.479	12.363	−12.841	−0.963
$Ti_3Al_{0.2}Sn_{0.8}C_2$	3.946	−0.577	12.309	−12.887	−0.955
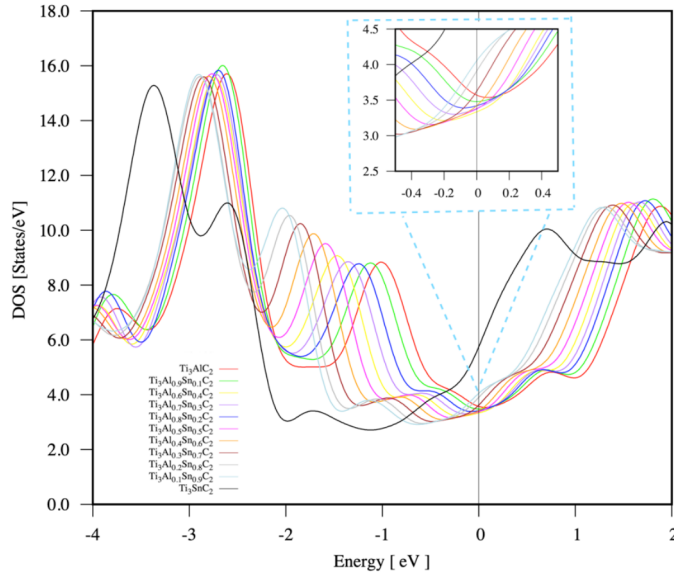
Figure 2. The calculated total density of states (TDOS) for $Ti_3Al_{1-x}Sn_xC_2$ (where x is ranging from 0 to 1 with interval 0.1) compositions.

The observed electronic band structure and the total density of states can be utilized to decide the electronic behavior of a solid crystal. In this view, to determine the electronic nature of the $Ti_3Al_{1-x}Sn_xC_2$

compounds, the energy band structures and the total density of electronic states were calculated and plotted along the high symmetry lines in the first Brillouin zone. The plotted electronic band structure was presented in Figure 3 for $Ti_3Al_{0.8}Sn_{0.2}C_2$ composition since it has same electronic behavior with other compositions. This similar electronic behavior could be seen from Figure 2. Also, it is concluded from Figure 3 that $Ti_3Al_{0.8}Sn_{0.2}C_2$ as well as these nanolaminated compositions are metals since there are no gaps between band branches around the Fermi level.

Furthermore, to understand the orbital dominancy on electronic nature for $Ti_3Al_{0.8}Sn_{0.2}C_2$ composition, the partial density of states (PDOS) and total density of states (TDOS) were given in Figure 4. It can be clearly seen in the figure that, especially in the conduction band which is above the Fermi energy level (E_F), there is a dominant contribution of the d-orbitals of titanium element (Ti) to the total density of states in these compositions. It can be said that, for the valence band below the Fermi energy level (E_F), the contribution from the p-orbitals of C atoms of $Ti_3Al_{0.8}Sn_{0.2}C_2$ is slightly more than the contributions from other orbitals of the other elements. In addition, s-orbitals of the atoms in these compositions have no significant effect on bonding properties and metallic character of these materials. This means that especially d-orbitals of titanium element (Ti) play a remarkable role on the electronic natures of the $Ti_3Al_{0.8}Sn_{0.2}C_2$ composition.

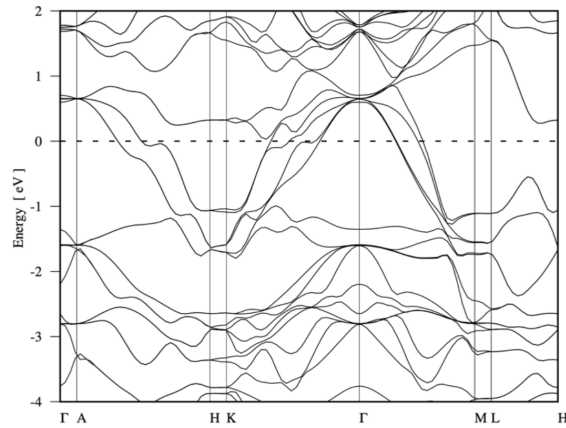**Figure 3**. The calculated energy band structure for $Ti_3Al_{0.8}Sn_{0.2}C_2$ compositions.

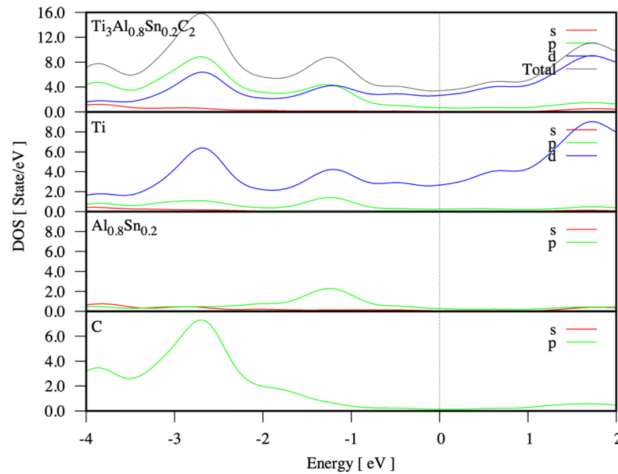**Figure 4**. The total density of states (TDOS) and the orbital projected partial density of electronic states (PDOS) for $Ti_3Al_{0.8}Sn_{0.2}C_2$ compositions.

4. Mechanical properties

The elastic constants of solid crystals establish a strong connection between their mechanical properties and their dynamic nature. They can also provide much information about the plastic deformation that can occur in their structures when an external force is applied. By using the optimized unit cells of these compositions, six independent elastic constants (C_{ij}) were calculated using the stress-strain method [37], and the calculated elastic constants for each composition having different *Sn* and *Al*-ratios are tabulated in Table 3. In technological applications, the mechanical stability of a solid, which is a desirable property for the sustainability, is defined as the resistance of the investigated crystal against external forces. Therefore, to be mechanically stable materials, their elastic constants should satisfy the Born-Huang criteria which are given below [38,39].

$$C_{11} - C_{12} > 0; \ C_{11} + 2C_{12} > 0; \ C_{33}\left(C_{11} + 2C_{12}\right) > 2C_{13}^2; \ C_{44} > 0$$

It can be concluded from Table 3 that $Ti_3 Al_{1-x} Sn_x C_2$ compositions have mechanical stability due to satisfying the Born–Huang criteria. Moreover, some mechanical properties of the $Ti_3 Al_{1-x} Sn_x C_2$ compositions were obtained using these constants.

Table 3. The calculated elastic constants ($\boldsymbol{C}_{ij}$ in *GPa*) and Cauchy pressures ($\boldsymbol{C}_p$ in *GPa*) of $Ti_3 Al_{1-x} Sn_x C_2$ compositions.

Compositions	C_{11}	C_{12}	C_{13}	C_{33}	C_{44}	C_{66}	C_p
Ti_3AlC_2	354.11	75.78	70.05	296.52	122.80	139.16	−47.02
	354*	76*	69*	296*	115*	139*	
$Ti_3Al_{0.9}Sn_{0.1}C_2$	354.80	76.26	70.97	299.94	120.68	139.27	−44.42
$Ti_3Al_{0.8}Sn_{0.2}C_2$	354.40	77.81	74.77	305.07	118.80	138.30	−40.99
$Ti_3Al_{0.7}Sn_{0.3}C_2$	352.05	79.63	75.89	305.67	120.98	136.21	−41.35
$Ti_3Al_{0.6}Sn_{0.4}C_2$	351.08	79.14	76.73	315.65	133.59	135.97	−54.45
$Ti_3Al_{0.5}Sn_{0.5}C_2$	349.11	81.96	77.35	314.20	124.70	133.58	−42.73
$Ti_3Al_{0.4}Sn_{0.6}C_2$	351.70	82.05	79.39	318.24	114.90	134.82	−32.85
$Ti_3Al_{0.3}Sn_{0.7}C_2$	349.35	82.50	79.78	314.11	105.73	133.43	−23.23
$Ti_3Al_{0.2}Sn_{0.8}C_2$	361.02	92.03	80.91	310.21	107.23	134.50	−15.20
$Ti_3Al_{0.1}Sn_{0.9}C_2$	335.13	92.54	80.40	307.41	102.70	121.30	−10.16
Ti_3SnC_2	326.63	89.16	80.30	300.20	103.27	118.73	−14.10
	328*	90*	76*	289*	103*	119*	

The resistance of a crystal with hexagonal symmetry against the changes in the main strain in the $[0\ 1\ \bar{1}\ 0]$ and $[0\ 0\ 0\ 1]$ directions can be deduced from the calculated C_{11} and C_{33} constants, respectively. For all compositions in this study, the calculated C_{11} constants are higher than C_{33} constants as listed in Table 3. This means that the incompressibility in the $[0\ 1\ \bar{1}\ 0]$ direction is stronger than in the $[0\ 0\ 0\ 1]$ direction [40]. Among the elastic constants, C_{66} and C_{44} can be defined as resistance to shear of the $\{1\ 0\ 0\}$ plane in the $<1\ 1\ 0>$ direction, and the resistance to shear of the $\{0\ 1\ 0\}$ or $\{1\ 0\ 0\}$ planes in the $<0\ 0\ 1>$ directions, respectively [41]. The C_{66} constants are higher than C_{44}, therefore these compounds are resistant to shear deformations of the $\{1\ 0\ 0\}$ plane in the $<1\ 1\ 0>$ direction. Moreover, the calculated elastic constants are consistent with the results obtained in previous studies.[1]

---

[1]*Materials Project (2020). mp-3747: $Ti_3 AlC_2$ [online]. Website https://materialsproject.org/materials/mp-3747/ and mp-21023: $Ti_3 SnC_2$ [online]. Website https://materialsproject.org/materials/mp-21023/ [accessed 29 December 2020].

The ductility or brittleness of a solid crystal could be determined with the Cauchy pressure (C_p) that can be calculated as $C_p = C_{12} - C_{44}$. The negative value of Cauchy pressure asserts that the brittleness of the interested solid [42]. As seen from Table 3, $Ti_3 Al_{1-x} Sn_x C_2$ compounds are brittle materials.

Some mechanical properties as listed in Table 4 can be predicted from the calculated elastic constants. Generally, the bulk modulus (B) of a crystal is defined as its resistance against change in its volume when a hydrostatic pressure is occurred on it while the resistance against its shape change is defined as the shear modulus (G). These properties could be predicted using the Voigt [43], Reuss [44] and Hill [45] approximations. The Voight approximation gives the upper limit for these properties while the Reuss approximation gives the lower limit. The Hill approximation takes the averages as listed in Table 4 and it provides to obtain these properties closer to the experimental results. As seen in this table, the predicted moduli (B and G) of $Ti_3 AlC_2$ and $Ti_3 SnC_2$ compositions are so close to the results in previous studies and also, the differences are only less than 5% between the obtained results and the previous studies. Furthermore, it is clear that as the doping rate of the tin (Sn) element in $Ti_3 Al_{1-x} Sn_x C_2$ compositions increases, the bulk modulus (B) tends to increase, while the shear modulus (G) decreases.

Table 4. The predicted bulk (B in GPa), shear (G in GPa) and Young's (E in GPa) moduli, G/B and B/G ratios, Poisson's ratio (ν) and Vickers hardness (H_V in GPa) for $Ti_3 Al_{1-x} Sn_x C_2$ compositions.

Compositions	B	E	G	ν	G/B	B/G	H_V
Ti_3AlC_2	159.01	305.01	129.21	0.18	0.81	1.23	14.28
		260[15]					11.40[15]
	159*		125*	0.19*			
$Ti_3Al_{0.9}Sn_{0.1}C_2$	160.12	304.16	128.51	0.18	0.80	1.25	14.14
$Ti_3Al_{0.8}Sn_{0.2}C_2$	162.76	302.82	127.24	0.19	0.78	1.28	14.05
		250[15]					10.20[15]
$Ti_3Al_{0.7}Sn_{0.3}C_2$	154.08	337.78	148.85	0.18	0.97	1.03	13.82
$Ti_3Al_{0.6}Sn_{0.4}C_2$	164.57	314.11	132.89	0.18	0.81	1.24	13.70
$Ti_3Al_{0.5}Sn_{0.5}C_2$	164.85	305.43	128.20	0.19	0.78	1.29	13.72
$Ti_3Al_{0.4}Sn_{0.6}C_2$	166.84	299.35	124.63	0.20	0.75	1.34	12.85
$Ti_3Al_{0.3}Sn_{0.7}C_2$	166.11	289.49	119.67	0.21	0.72	1.39	12.57
$Ti_3Al_{0.2}Sn_{0.8}C_2$	170.54	293.51	120.97	0.21	0.71	1.41	12.68
$Ti_3Al_{0.1}Sn_{0.9}C_2$	164.68	276.36	113.23	0.22	0.69	1.45	12.61
Ti_3SnC_2	161.24	272.24	111.70	0.22	0.69	1.44	12.23
	158*		112*	0.21*			

*Materials Project (2020). mp-3747: $Ti_3 AlC_2$ [online].
Website https://materialsproject.org/materials/mp-3747/ and mp-21023: $Ti_3 SnC_2$ [online].
Website https://materialsproject.org/materials/mp-21023/ [accessed 29 December 2020].

Among the estimated some mechanical parameters, Young's modulus (E) calculated as the ratio of stress and strain can be used to define the linear strain along edges [46]. These compositions have high stiffness due to the high Young's modulus (E) as listed in Table 4. Furthermore, B/G values which are known as Pugh ratios [47] can be used to estimate the ductility or brittleness behavior of solids. Accordingly, if the calculated B/G value is greater than the critical number as 1.75 [48], a solid crystal with this value may be expected to exhibit ductile behavior, otherwise brittle. In this regard, the presented compositions in this study are brittle materials and this result is coherent with the Cauchy pressures. The G/B ratio is a crucial parameter to establish the dominant bonding type of a crystal and it can be said that, if the obtained value is about 1.1, the dominancy of

the covalent bonding in a crystal is greater than the other bonding types. On the other hand, it can be estimated that, if the mentioned value of a solid is around 0.6, the atomic bonding character is ionic [46]. As a result, the G/B ratios theoretically calculated in the present study support the ionic contribution in $Ti_3 Al_{1-x} Sn_x C_2$ compositions.

The compressibility or incompressibility of the material can be determined using the calculated Poisson's ratio (ν) [49] and according to this view, if this ratio of any crystal approaches to value of 0.5, the mentioned material shows incompressible character. In this study, it is obvious from the Table 4 that the calculated Poisson's ratios for the present compositions are close to 0.2 value indicating their compressibility nature. Additionally, this ratio can be an indicator for the characteristics of the bonding types in solids and the known typical value to verify ionic character is 0.25 whereas 0.1 value shows covalent type [35,50]. In this respect, the types of bonding of these compounds are ionic, in accordance with the G/B ratios previously presented.

Moreover, the Vickers hardness (H_V) from the semiempirical method [51] were used to define the hardness of the compositions and the calculated values were tabulated in Table 4. As seen in the table, the obtained hardness values for $Ti_3 AlC_2$ and $Ti_3 Al_{0.8} Sn_{0.2} C_2$ compositions are consistent with the literature [15]. In addition, the $Ti_3 Al_{1-x} Sn_x C_2$ compositions can be defined as hard material since the calculated hardness values are in between 10 GPa and 40 GPa.

The three-dimensional and two-dimensional Young's modulus, linear compressibility, shear modulus and Poisson's ratio of $Ti_3 Al_{0.8} Sn_{0.2} C_2$ composition were visualized as seen in Figures 5a–5d (to save space in this paper, the figures of $Ti_3 Al_{0.8} Sn_{0.2} C_2$ composition are presented which is a focal point of this study, since other compositions show similar behaviors). In these figures, the green shapes show the minimum values whereas the blue ones show the maximum values. As seen in Figure 5, these properties are isotropic in xy plane while the anisotropic character could be observed in yz and xz planes.

Additionally, the sound wave velocities depended on direction and the related phase polarization and power flow angle were plotted with the help of Christoffel tool in which the elastic stiffness constants and the density of material are used, as presented in Figures 6a–6d. The fast and slow secondary modes correspond to the transverse wave velocities while the primary mode corresponds to the longitudinal wave velocity. In the figures, it is clearly seen that the observed group and phase velocities have relatively smaller values in z-axis. However, in x- and y-axes, the fast and the primary modes have higher values whereas the slow secondary mode has lower values in the same axes. In Figure 6c, similar behaviors for x-, y- and z-axes are seen in phase polarization too. Also, the primary mode has transverse polarization in all planes while the slow secondary mode has transverse polarization in all directions and the fast secondary mode has longitudinal polarization in x and y directions and transverse in z directions. The power flow angle being the angle between the group wave velocity and the phase wave velocity has lowest values in all axes, as seen in Figure 6d.

5. Conclusion

$Ti_3 Al_{1-x} Sn_x C_2$ with x ranging from 0 to 1 with 0.1 interval was studied using CASTEP program package. The structural optimizations were revealed that these compositions are thermodynamically stable. Also, the general trend of the lattice constants with the Sn addition was rising. Also, it was found that these compositions have metallic character and the band filling theory was revealed that the most stable structure among these compounds is $Ti_3 Al_{0.8} Sn_{0.2} C_2$. The mechanical stability of these compositions was determined with the elastic stiffness matrix. Moreover, the calculated elastic constants were used to obtain the mechanical properties such as bulk modulus, Poisson's ratio, etc. As the Sn doping increases, the bulk modulus increases while the shear
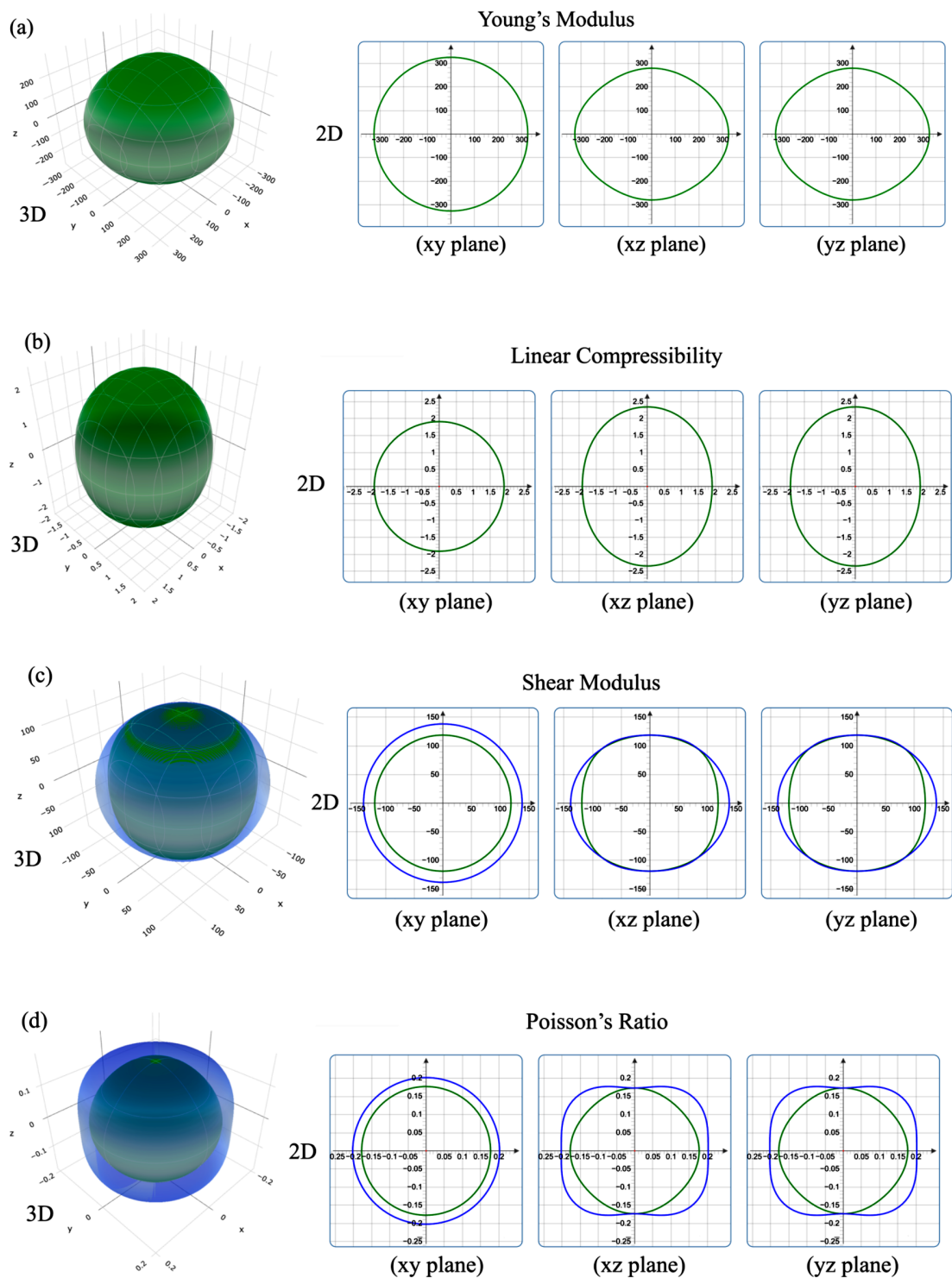
Figure 5. (a) Young's modulus, (b) linear compressibility, (c) shear modulus, and (d) Poisson's ratio for $Ti_3 Al_{0.8} Sn_{0.2} C_2$ composition in 3-D and 2-D.
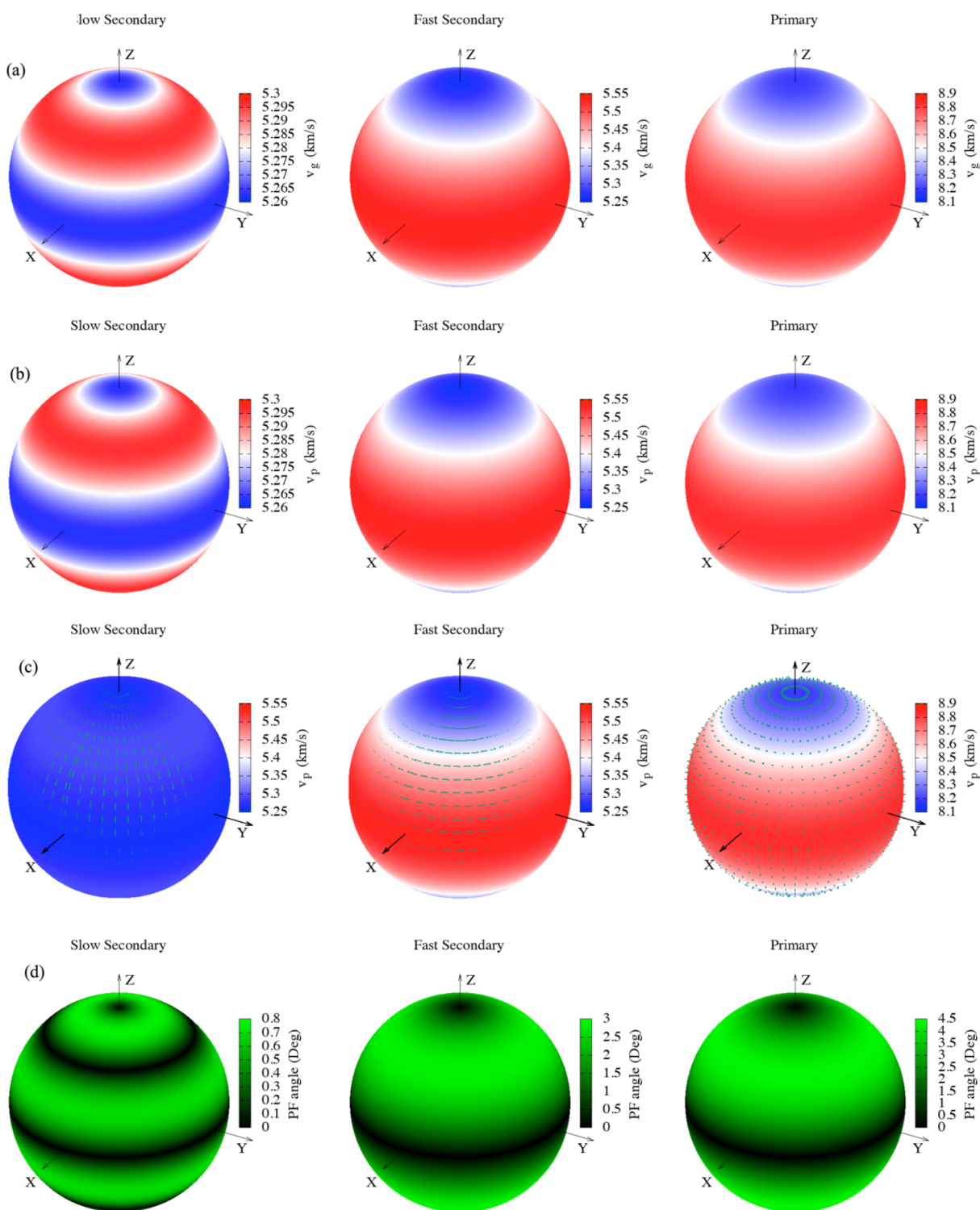
Figure 6. The directional dependent (a) group velocity, (b) phase velocity, (c) phase polarization, and (d) power flow angle for $Ti_3 Al_{0.8} Sn_{0.2} C_2$ composition.

modulus decreases. Also, all these compositions are brittle materials. In addition, the isotropic nature of Young's modulus, linear compressibility, shear modulus and Poisson's ratio in xy plane is found while these properties are anisotropic in yz and xz planes. The sound wave velocities in 3D were obtained and it was found that the observed group and phase velocities have relatively smaller values in z-axis. This study presents the detailed electronic and mechanic properties of Sn doped $Ti_3Al_{1-x}Sn_xC_2$ compounds where Sn atoms could result from the experimental synthesis procedure and it could have a potential to lead the future studies.

Acknowledgment

References

1 Barsoum MW. $M_{n+1}AX_n$ phases: a new class of solids; thermodynamically stable nanolaminates. Progress in Solid State Chemistry 2000; 28: 201-281. doi: 10.1016/S0079-6786(00)00006-6

2 Sokol M, Natu V, Kota S, Barsoum MW. On the chemical diversity of the MAX phases. Trends in Chemistry 2019; 1: 210-223. doi: 10.1016/j.trechm.2019.02.016

3 Bai Y, Srikanth N, Chua CK, Zhou K. Density functional theory study of $M_{n+1}AX_n$ phases: a review. Critical Reviews in Solid State and Materials Sciences 2019; 44: 56-107. doi: 10.1080/10408436.2017.1370577

4 Surucu G, Gencer A, Wang X, Surucu O. Lattice dynamical and thermo-elastic properties of M_2AlB (M = V, Nb, Ta) MAX phase borides. Journal of Alloys and Compounds 2020; 819: 153256. doi: 10.1016/j.jallcom.2019.153256

5 Mingxing A, Hongxiang Z, Yang Z, Zhaoyun T, Zhenying H et al. Synthesis of Ti_3AlC_2 powders using Sn as an additive. Journal of the American Ceramic Society 2006; 89: 1114-1117. doi: 10.1111/j.1551-2916.2005.00818.x

6 Zhai HX, Huang ZY, Zhou Y, Zhang ZL, Li SB et al. Ti_3AlC_2- a soft ceramic exhibiting low friction coefficient. Materials Science Forum 2005; 475-479: 1251-1254. doi: 10.4028/www.scientific.net/msf.475-479.1251

7 Chen W, Tang J, Shi X, Ye N, Yue Z et al. Synthesis and formation mechanism of high-purity Ti_3AlC_2 powders by microwave sintering. International Journal of Applied Ceramic Technology 2020; 17: 778-789. doi: 10.1111/ijac.13452

8 Zhu J, Mei B, Xu X, Liu J. Synthesis of single-phase polycrystalline Ti3SiC2 and Ti_3AlC_2 by hot pressing with the assistance of metallic Al or Si. Materials Letters 2004; 58: 588-592. doi: 10.1016/S0167-577X(03)00567-6

9 Zhou W, Mei B, Zhu J, Hong X. Synthesis of high-purity Ti3SiC2 and Ti_3AlC_2 by spark plasma sintering (SPS) technique. Journal of Materials Science 2005; 40: 2099-2100. doi: 10.1007/s10853-005-1245-z

10 Zou Y, Sun ZM, Tada S, Hashimoto H. Synthesis reactions for Ti_3AlC_2 through pulse discharge sintering $Ti/A1_4C_3/TiC$ powder mixture. Scripta Materialia 2006; 55: 767-770. doi: 10.1016/j.scriptamat.2006.07.018

11 Zou Y, Sun ZM, Tada S, Hashimoto H. Rapid synthesis of single-phase Ti_3AlC_2 through pulse discharge sintering a $TiH_2/Al/TiC$ powder mixture. Scripta Materialia 2007; 56: 725-728. doi: 10.1016/j.scriptamat.2007.01.026

12 Yeh CL, Shen YG. Combustion synthesis of Ti_3AlC_2 from Ti/Al/C/TiC powder compacts. Journal of Alloys and Compounds 2008; 466: 308-313. doi: 10.1016/j.jallcom.2007.11.037

13 Wang X, Zhou Y. Solid-liquid reaction synthesis of layered machinable Ti_3AlC_2 ceramic. Journal of Materials Chemistry 2002; 12: 455-460. doi: 10.1039/b108685e

14 Han JH, Hwang SS, Lee D, Park SW. Synthesis and mechanical properties of Ti_3AlC_2 by hot pressing TiC_x/Al powder mixture. Journal of European Ceramic Society 2008; 28: 979-988. doi: 10.1016/j.jeurceramsoc.2007.09.015

15 Bei GP, Gauthier-Brunet V, Tromas C, Dubois S. Synthesis, Characterization, and intrinsic hardness of layered nanolaminate Ti_3AlC_2 and $Ti_3Al_{0.8}Sn_{0.2}C_2$ solid solution. Journal ofthe American Ceramic Society 2012; 95: 102-107. doi: 10.1111/j.1551-2916.2011.04846.x

16 Hongxiang Z, Zhenying H, Mingxing A, Yang Z, Zhili Z et al. Tribophysical properties of polycrystalline bulk Ti_3AlC_2. Journal of the American Ceramic Society 2005; 88: 3270-3274. doi: 10.1111/j.1551-2916.2005.00588.x

17 Li SB, Zhai HX, Bei GP, Zhou Y, Zhang ZL. Formation of Ti_3AlC_2 by mechanically induced self-propagating reaction in Ti-Al-C system at room temperature. Materials Science and Technology 2006; 22: 667-672. doi: 10.1179/174328406X91050

18 Drouelle E, Brunet V, Cormier J, Villechaise P, Sallot P et al. Oxidation resistance of Ti_3AlC_2 and $Ti_3Al_{0.8}Sn_{0.2}C_2$ MAX phases: a comparison. Journal of the American Ceramic Society 2020; 103: 1270-1280. doi: 10.1111/jace.16780

19 Li S, Xiang W, Zhai H, Zhou Y, Li C et al. Formation of a single-phase Ti_3AlC_2 from a mixture of Ti, Al and TiC powders with Sn as an additive. Materials Research Bulletin 2008; 43: 2092-2099. doi: 10.1016/j.materresbull.2007.09.016

20 Peng CQ, Wang CA, Qi L, Huang Y. Fabrication of Ti_3AlC_2 Ppowder with high-purity by pressureless sintering. Materials Science Forum 2005; 475-479: 1247-1250. doi: 10.4028/www.scientific.net/msf.475-479.1247

21 Bei GP, Laplanche G, Gauthier-Brunet V, Bonneville J, Dubois S. Compressive behavior of Ti_3AlC_2 and $Ti_3Al_{0.8}Sn_{0.2}C_2$ MAX phases at room temperature. Journal of the American Ceramic Society 2013; 96: 567-576. doi: 10.1111/jace.12092

22 Clark SJ, Segall MD, Pickard CJ, Hasnip PJ, Probert MIJ et. al. First principles methods using CASTEP. Zeitschrift für Kristallographie 2005; 220: 567-570. doi: 10.1524/zkri.220.5.567.65075

23 Perdew JP, Burke K, Ernzerhof M. Generalized gradient approximation made simple. Physical Review Letters 1996; 77: 3865-3868. doi: 10.1103/PhysRevLett.77.3865

24 Perdew JP, Chevary JA, Vosko SH, Jackson KA, Pederson MR et al. Atoms, molecules, solids, and surfaces: applications of the generalized gradient approximation for exchange and correlation. Physical Review B 1992; 46: 6671-6687. doi: 10.1103/PhysRevB.46.6671

25 Zhu W, Xiao H. Ab initio study of electronic structure and optical properties of heavy-metal azides: TlN_3, AgN_3, and CuN_3. Journal of Computational Chemistry 2008; 29: 176-184. doi: 10.1002/jcc.20682

26 Hammer B, Hansen LB, Nørskov JK. Improved adsorption energetics within density-functional theory using revised Perdew-Burke-Ernzerhof functionals. Physical Review B - Condensed Matter and Material Physics 1999; 59: 7413-7421. doi: 10.1103/PhysRevB.59.7413

27 Bellaiche L, Vanderbilt D. Virtual crystal approximation revisited: Application to dielectric and piezoelectric properties of perovskites. Physical Review B - Condensed Matter and Material Physics 200; 61: 7877-7882. doi: 10.1103/PhysRevB.61.7877

28 Gaillac R, Pullumbi P, Coudert FX. ELATE: An open-source online application for analysis and visualization of elastic tensors. Journal of Physics: Condensed Matter 2016; 28: 275201. doi: 10.1088/0953-8984/28/27/275201

29 Jaeken JW, Cottenier S. Solving the Christoffel equation: phase and group velocities. Computer Physics Communications 2016; 207: 445-451. doi: 10.1016/j.cpc.2016.06.014

30 Fedorov FI. General equations of the theory of elasticity. In: Theory Elastic Waves in Crystals. New York, NY, USA: Springer, 1968, pp. 1-33. doi: 10.1007/978-1-4757-1275-9_1

31 Surucu G, Yildiz B, Erkisi A, Wang X, Surucu O. The investigation of electronic, anisotropic elastic and lattice dynamical properties of MAB phase nanolaminated ternary borides: M_2AlB_2 (M=Mn, Fe and Co) under spin effects. Journal of Alloys and Compounds 2020; 838: 155436. doi: 10.1016/j.jallcom.2020.155436

32 Xu JH, Oguchi T, Freeman AJ. Crystal structure, phase stability, and magnetism in Ni_3V. Physical Review B 1987; 35: 6940-6943. doi: 10.1103/PhysRevB.35.6940

33 Xu JH, Freeman AJ. Band filling and structural stability of cubic trialuminides: YAl_3, $ZrAl_3$, and $NbAl_3$. Physical Review B 1989; 40: 11927-11930. doi: 10.1103/PhysRevB.40.11927

34 Surucu G, Erkisi A. An ab initio study on the investigation of structural, electronic, mechanical and lattice dynamical properties of the M_2AX type MAX phases $Sc_2AlB_{0.5}C_{0.5}$, $Sc_2AlB_{0.5}N_{0.5}$ and $Sc_2AlC_{0.5}N_{0.5}$ compounds. Materials Research Express 2017; 4: 106520. doi: 10.1088/2053-1591/aa9282

35 Surucu G. Investigation of structural, electronic, anisotropic elastic, and lattice dynamical properties of MAX phases borides: an Ab-initio study on hypothetical M_2AB (M = Ti, Zr, Hf; A = Al, Ga, In) compounds. Materials Chemistry and Physics 2018; 203: 106-117. doi: 10.1016/j.matchemphys.2017.09.050

36 Surucu G, Kaderoglu C, Deligoz E, Ozisik H. Investigation of structural, electronic and anisotropic elastic properties of Ru-doped WB_2 compound by increased valence electron concentration. Materials Chemistry and Physics 2017; 189: 90-95. doi: 10.1016/j.matchemphys.2016.12.036

37 Nye JF. Physical Properties of Solid Crystals. 1st ed. Oxford, UK: Claredon, 1957.

38 Born M. On the stability of crystal lattices I. Mathematical Proceedings of the Cambridge Philosophical Society 1940; 36: 160-172. doi: 10.1017/S0305004100017138

39 Mouhat F, Coudert FX. Necessary and sufficient elastic stability conditions in various crystal systems. Physical Review B - Condensed Matter and Material Physics 2014; 90: 224104. doi: 10.1103/PhysRevB.90.224104

40 Surucu G, Colakoglu K, Deligoz E, Korozlu N. First-principles study on the MAX phases $Ti_{n+1}GaN_n$ (n = 1,2, and 3). Journal of Electronic Materials 2016; 45: 4256-4264. doi: 10.1007/s11664-016-4607-1

41 Feng W, Cui S. Mechanical and electronic properties of Ti_2AlN and Ti_4AlN_3: A first-principles study. Canadian Journal of Physics 2014; 92: 1652-1657. doi: 10.1139/cjp-2013-0746

42 Pettifor DG. Theoretical predictions of structure and related properties of intermetallics. Materials Scienace and Technology 1992; 8: 345-349. doi: 10.1179/mst.1992.8.4.345

43 Voigt W. Lehrbuch der Kristallphysik. Berlin, Germany: Vieweg+Teubner Verlag, 1966 (in German). doi: 10.1007/978-3-663-15884-4

44 Reuss A. Berechnung der fließgrenze von mischkristallen auf grund der plastizitätsbedingung für einkristalle. Zeitschrift für Angewandte Mathematik und Mechanik 1929; 9: 49-58 (in German). doi: 10.1002/zamm.19290090104

45 Hill R. The elastic behaviour of a crystalline aggregate. Proceedings of the Physical Society Section A 1952; 65: 349-354. doi: 10.1088/0370-1298/65/5/307

46 Surucu G, Gullu HH, Candan A, Yildiz B, Erkisi A. First-principles studies of $Ti_{n+1}SiN_n$ (n=1, 2, 3) MAX phase. Philosophical Magazine 2020; 100: 2183-2204. doi: 10.1080/14786435.2020.1759835

47 Pugh SF. XCII. Relations between the elastic moduli and the plastic properties of polycrystalline pure metals.The London, Edinburgh, and Dublin Philosophical Magazine and Journal of Science 1954; 45: 823-843. doi: 10.1080/14786440808520496

48 Surucu G, Colakoglu K, Deligoz E, Ciftci YO. Structural, electronic and mechanical properties of $W_{1-x}Tc_xB_2$ alloys. Solid State Communications 2013; 17: 1-4. doi: 10.1016/j.ssc.2013.07.002

49 Sin'ko GV, Smirnov NA. Ab initio calculations of elastic constants and thermodynamic properties of bcc, fcc, and hcp Al crystals under pressure. Journal of Physics: Condensed Matter 2002; 14: 6989-7005. doi: 10.1088/0953-8984/14/29/301

50 Bannikov VV, Shein IR, Ivanovskii AL. Electronic structure, chemical bonding and elastic properties of the first thorium-containing nitride perovskite $TaThN_3$. Physica Status Solidi - Rapid Research Letters 2007; 1: 89-91. doi: 10.1002/pssr.200600116

51 Lyakhov AO, Oganov AR. Evolutionary search for superhard materials: Methodology and applications to forms of carbon and TiO_2. Physical Review B - Condensed Matter and Material Physics 2011; 84: 092103. doi: 10.1103/PhysRevB.84.092103